Miniature tensile testing of SPD processed fine-grained aluminum

Lanjewar, Harishchandra A.; Naghdy, Soroosh; Kestens, Leo A.I.; Verleysen, Patricia

Citation (APA)
Lanjewar, H. A., Naghdy, S., Kestens, L. A. I., & Verleysen, P. (2019). Miniature tensile testing of SPD processed fine-grained aluminum. *Journal of Physics: Conference Series*, *1270*(1), Article 012022. https://doi.org/10.1088/1742-6596/1270/1/012022

Important note
To cite this publication, please use the final published version (if applicable).
Please check the document version above.

PAPER • OPEN ACCESS

Miniature tensile testing of SPD processed fine-grained aluminum

To cite this article: Harishchandra A Lanjewar *et al* 2019 *J. Phys.: Conf. Ser.* **1270** 012022

View the article online for updates and enhancements.

IOP **ebooks**™

Bringing you innovative digital publishing with leading voices to create your essential collection of books in STEM research.

Start exploring the collection - download the first chapter of every title for free.

Miniature tensile testing of SPD processed fine-grained aluminum

Harishchandra A Lanjewar[1,*], Soroosh Naghdy[1,2], Leo A I Kestens[1,3] and Patricia Verleysen[1]

[1]Department of Electrical Energy, Metals, Mechanical Construction and Systems (EEMMeCS), Ghent University, Ghent, Belgium
[2]Process models, ArcelorMittal, Ghent, Belgium
[3]Department of Materials Science and Engineering, Delft University of Technology, Delft, The Netherlands

*E-mail: harishchandra.lanjewar@ugent.be

Abstract. Manufacturing of ultrafine-grained (UFG) or nanocrystalline (NC) metals via a single step top-down approach imposing severe plastic deformation (SPD) is one of the most promising ways to achieve superior properties such as high strength and superplastic forming capability. Nonetheless, the lack of relevant data on their post-SPD performance in different test environments makes it difficult to fully understand their mechanical behavior. While characterizing the tensile behavior, almost all of the previous reports are limited to the discussion on the plastic performance of the material in terms of elongation to failure and corresponding strength, with only a few studies discussing the effect of grain fragmentation on work hardening response of the material. In the present work, a comprehensive analysis is presented in terms of the uniform and post-necking mechanical behavior of the ultrafine-grained material. Commercially pure aluminum is subjected to high pressure torsion (HPT) deformation with strains ranging from very low levels ($\gamma \approx 2.1$) to values well in the saturation regime ($\gamma \approx 25.1$). When tested in uniaxial tension, the strength increases monotonously. The uniform elongation improves with the imposed HPT strain, though remains lower than the value of the initial material. Based on the slopes of the stress-strain curve, three distinct zones are identified, i.e. uniform deformation, post-necking-1, and post-necking-2. With accumulating SPD deformation, the material shows enhanced pre-necking strength and ductility; while post-necking material fails early and at lower strength levels. The post-necking response is observed to be highly microstructure dependent: a lower grain size augments the resistance for micro-crack propagation and thus the ductility, however, once initiated, a crack propagates much faster in fine-grained than in coarse-grained HPT processed material.

1. Introduction

Fabrication of ultrafine-grained (UFG) or nanocrystalline (NC) metals via single step top-down approaches imposing severe plastic deformation (SPD) is one of the most promising ways to achieve superior properties such as high strength and superplastic forming capability [1]. Over the last two decades, many studies have been conducted on a variety of metals. Three methods, namely equal channel angular pressing (ECAP) [2], accumulative roll bonding (ARB) [3] and high pressure torsion (HPT) [4] have emerged as the most potent tools to generate refined structures. ECAP and ARB

requires multiple passes to impose large plastic strains on the material, contrary to HPT where a significant amount of strain can be imposed on a disk-shaped sample in one single operation. Thus produced nanostructured (NS)/ultrafine-grained (UFG) metals, quite independent of the processing route, when tested in tension after pre-straining in simple shear mode, show extraordinary enhancements in strength but suffer from poor ductility [5]. However, with continued shear straining the uniform deformation improves to some extent and has been associated with the smaller size of the nucleating flaws during plastic instability [6]. In the case of ECAP Cu, increased rate sensitivity owing to refined grain size has been considered another contributing factor to improved ductility [7]. Methods to improve upon the combination of strength-ductility property have been proposed by either engineering a multi-component structure or post-SPD treatments [8]. In post-SPD annealing treatments, work hardening capacity of the material was seen to improve in conjunction with the reduction in overall dislocation density [9]. During such annealing treatments, non-equilibrium boundaries which are known to be present in large proportions in SPD material, convert into boundaries of equilibrium nature, i.e. with lowered geometrically necessary dislocation density and thereby enhanced ability to store the deformation [10].

In present work, the mechanical behavior of UFG metal is studied using uniaxial tensile testing of miniature dog-bone shaped specimen extracted from HPT deformed commercially pure aluminum (CP Al). The HPT deformation includes very small strains as well as strains in the saturation regime so that a continuous progression in the grain structure is obtained and later linked to their plastic flow properties in terms of elongation, strength and work hardening behavior. Based on the uniform deformation and post-necking mechanical behavior, preliminary conclusions can be drawn about the potential failure conditions specific to the UFG metals.

2. Material and methods

The cast block material of CP Al (Al - 99.6 wt%) was cold rolled to a thickness of 1.3 mm and annealed at 773 K for 30 s, producing an average grain size of 85 μm. HPT was performed, using 15 mm disks punched out of the annealed sheet, at a nominal pressure of 2.5 GPa and different rotations of ¼, ½, 2 and 3, at a rotational speed of 1 rpm. The equivalent strain applied during HPT is calculated using relation [11]:

$$\varepsilon_{eq} = \frac{r\varphi}{3^{1/2}h} \qquad (1)$$

where r is the sample radius, φ is the rotation applied in rad and h is the sample initial thickness. As shown in figure 1 (a), two dog-bone shaped miniature tensile samples were extracted from each HPT processed disk using electrical discharge machining (EDM). The simple shear deformation geometry in terms of directions - radial (r), shear (θ) and shear plane normal (z) is also indicated.
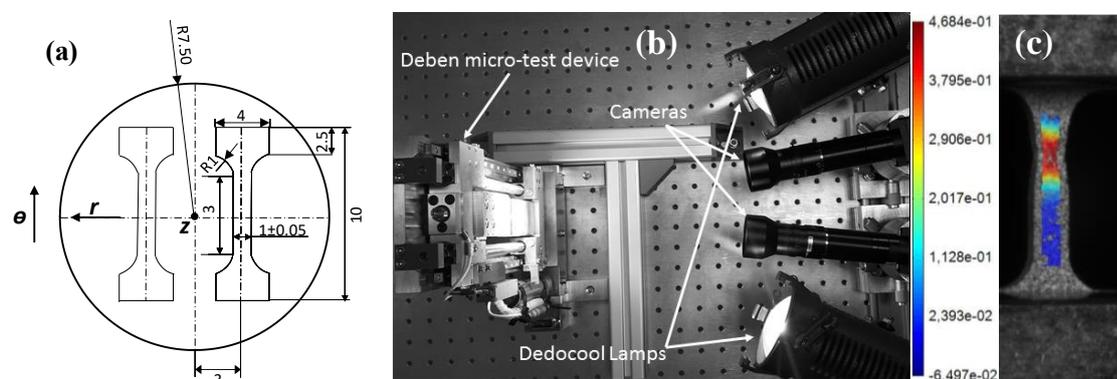

Figure 1. (a) Tensile sample extraction scheme with simple shear geometry, (b) tensile test and camera setup during an experiment and (c) full-field strain map using 3-dimensional digital image correlation (3D DIC).

The HPT ε_{eq} in the center of the tensile samples was 2.1, 4.2, 16.7, and 25.1. In addition, annealed material was also tested along different orientations with respect to the rolling direction, i.e. 0°, 45°, and 90°. A dual-screw Deben® micro-test device with 1 kN load cell was used and tests were performed at a strain rate of 0.0056 s^{-1}. For full-field strain mapping, 3D DIC a non-contact optical strain measurement technique was used. Here the tensile samples were spray painted with the speckle pattern (black dots over white background). Two high-resolution cameras captured the images of the deforming specimen during tension tests (figure 1 (b) and (c)). MacthID Grabber® was used to acquire the force and camera signals, while subsequent image correlations and calculations were performed using MatchID Stereo®, both are the modules of the commercial DIC software package MatchID®.

The microstructural characterization was carried out using electron backscatter diffraction (EBSD) in a scanning electron microscope (SEM) with a field emission gun (FEG). The observations were performed on the *r-θ* plane. During the analysis to determine the average grain size (*GS*), using OIM^{TM} software, 1° and 15° were chosen as the minimum boundary misorientation and high angle boundary misorientation, respectively.

3. Experimental results and discussion

The microstructure experiences refinement in *GS* with the accumulating HPT strain and reduces to average values of 48, 18, 1.22, and 1.42 μm at ε_{eq} of 2.8, 4.2, 16.7, and 27.9, respectively. The engineering strain is obtained by calculating the extension between two horizontal lines marking the gage length of the specimen. The engineering stress-strain curves for annealed material along different orientations are shown in figure 2 (a). Generally, to describe the stress-strain behavior in metals Hollomon's power law can be used and in that case, the work hardening rate is given by:
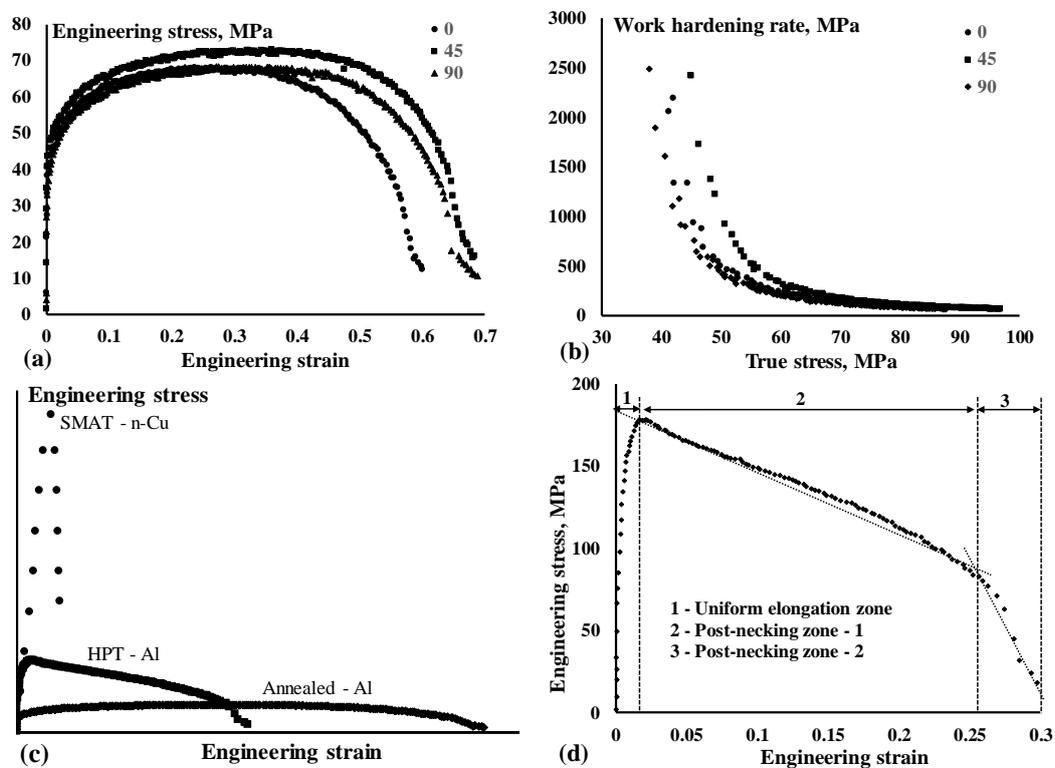

Figure 2. Engineering stress-strain curves (a) and work hardening rates along different orientations (b) for annealed material. (c) Engineering stress-strain curves for nano-Cu (*n*-Cu) from ref [12], annealed and HPT processed Al from present work and (d) partitioned engineering stress-strain curve for HPT Al.

$$\frac{d\sigma}{d\varepsilon} = n\frac{\sigma}{\varepsilon} \qquad (2)$$

where n is the strain hardening exponent, σ is the true stress and ε is the true strain. In the annealed material a slight anisotropy can be observed in both (figure 2 (b)), stress-strain and work hardening response. The material shows *stage III* and *IV* of work hardening. In *stage III* a rapid decline in work hardening is manifested due to the balance between dislocation multiplication and local dislocation annihilation process [13]. On the other hand, in *stage IV* where the work hardening rate is constant, the microstructure breaks into localized bands leading to deformation concentration in such bands.

Various studies conducted to evaluate the tensile properties of NC/UFG metals have reported two types of mechanical behavior with regard to the post-necking elongation, as shown by *n*-Cu from ref [12] and HPT-Al from present work, in figure 2 (c) [8, 12]. Though both show lower uniform elongation after reaching maximum load, *n*-Cu fails soon while HPT Al shows long tail-like post-necking elongation. As shown in figure 2 (d), the engineering stress-strain curve for HPT Al can be partitioned into three distinct zones: (i) uniform deformation zone (UEZ), (ii) post-necking zone-1 (PNZ-1), and (iii) post-necking zone-2 (PNZ-2). The PNZ-1 demarcates the diffuse necking deformation, whereas PNZ-2 covers the localized elongation in a very narrow band preceding failure.

The true stress-strain values for both the homogeneous and post-necking tensile deformation for HPT Al are shown in figure 3. As can be seen, the stress-strain values corresponding to the yielding and maximum load conditions show continuous improvement with ε_{eq}. The 0.2% offset yield strength which is ~42 MPa in annealed condition reaches a value of 146 MPa at ε_{eq} of 25.1. Contrary to the conventional forming processes, here in HPT, uniform deformation increase with accumulating shear strain in the material. Unlike pre-necking stress-strain values, the true stress values corresponding to the end of PNZ-1(σ_p) and PNZ-2(σ_f), either stay constant or decrease, respectively. To further compare

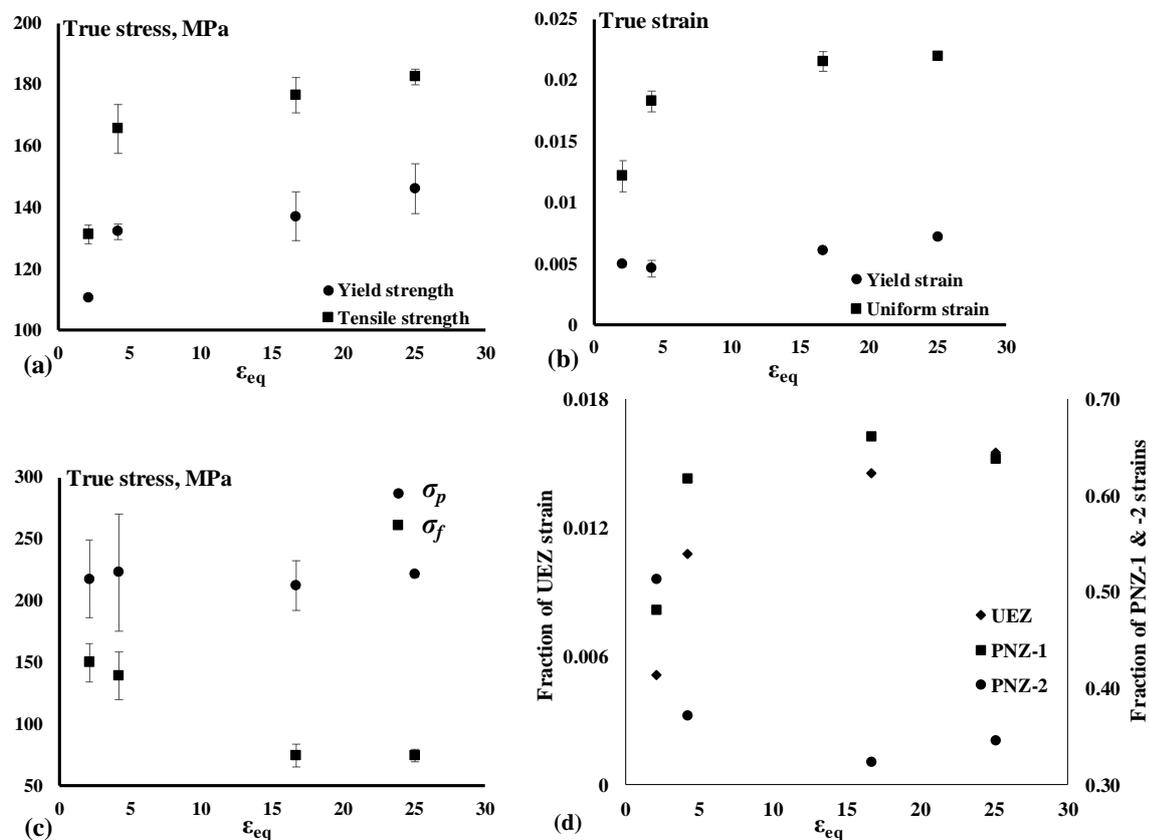**Figure 3.** True yield and tensile stress (a) and strain (b) values; true stress values corresponding to the end of PNZ-1 (σ_p) and –2 (σ_f) and (d) true strain fractions from each of the deformation zone.

the pre- and post-necking tensile behavior, the average true strain values are utilized to determine the strain fractions from each deformation zone as shown in figure 3 (d). The true strain corresponding to the end of PNZ-1 is obtained from the volume constancy using the width strain value from a local strain field correlation near the fracture; while that for PNZ-2 is obtained from topographic measurements using SEM. From figure 3 (d), it can be observed that both UEZ and PNZ-1 strain fractions increase, while the strain fractions corresponding to PNZ-2 decrease with ε_{eq}. Thus it can be concluded that with ε_{eq} and refining GS, the pre-necking plastic performance improves, while post-necking plasticity deteriorates on account of the lower local ductility values.

Chan reported that in the case of fine-grained material, the stress required for micro-crack nucleation is lower than that required for propagation and therefore additional plastic work is required for crack propagation [14]. In present work, much better ductility observed in PNZ-1 indicates its role in providing the necessary plastic deformation and thereby strain hardening to locally produce the stress concentrations favorable for micro-crack propagation. This plastic work increases with decreasing grain size indicating an important role played by the refining GS in delaying the fracture. However, once initiated the finer-grained material fractures more swiftly than their coarse-grained counterparts.

The work hardening rates for HPT processed material are calculated using equation (2) and are plotted vs. true stress in figure 4 (a), while the linear slopes of the work hardening rates at different ε_{eq} are shown in figure 4 (b). It can be seen that unlike annealed material which exhibits both *stage III* and *IV* work hardening, HPT processed material shows only *stage III* hardening. The work hardening in severely deformed structures becomes difficult due to the presence of a large fraction of non-equilibrium boundaries which are known to possess enhanced diffusion properties [15]. In addition, dissociation of trapped dislocations at non-equilibrium boundaries is considered as one of the prevalent recovery mechanism in SPD processed materials [16-17]. However, from figure 4 (d) it can be seen that the work hardening ability is improving with ε_{eq}, which seems to be the source of enhancing uniform deformation in figure 3 (b).
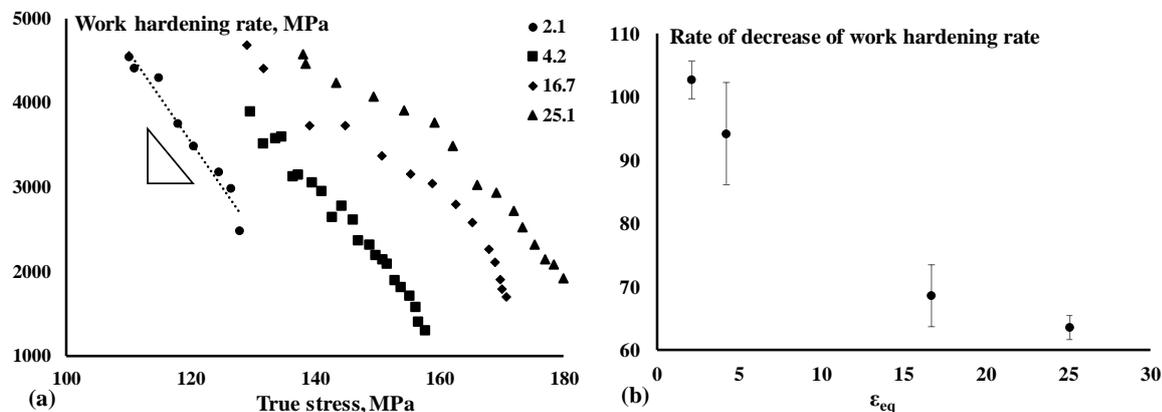

Figure 4. (a) Work hardening rates calculated for HPT processed material plotted vs. true stress and (b) the slope of *stage III* work hardening vs. ε_{eq}.

4. Conclusions
From the above experimental results and discussion following conclusions can be drawn:

1) The rolled and recrystallized material shows a slight anisotropy in its stress-strain and work hardening response. The annealed material exhibits *stage III* and *IV* hardening, while HPT processed material owing to efficient recovery mechanisms possess only *stage III* hardening.

2) With ε_{eq}, the pre-necking plastic properties show improvement, while the post-necking plastic performance deteriorates owing to reduced local ductility.

3) Refining *GS* causes the plastic work required for micro-crack propagation to increase and thereby delays the fracture. However, once initiated the finer-grained material fractures rapidly.

4) The work hardening ability of SPD processed material improves with the accumulating shear deformation.

References
[1]   Zhilyaev A P and Langdon T G 2008 *Prog. Mater. Sci.* **53** 893-979
[2]   Valiev R Z and Langdon T G 2006 *Progr. Mater. Sci.* **51** 881-981
[3]   Pirgazi H and Akbarzadeh A 2008 Int. J. Mod. Phys. B **22** 2840-47
[4]   Naghdy S, Kestens L, Hertelé S and Verleysen P 2016 *Mater. Charact.* **120** 285-94
[5]   Dalla Torre F H, Lapovok R, Sandlin J, Thomson P F, Davies C H J and Pereloma E V 2004 *Acta Mater.* **52** 4819-32
[6]   Wang Y M, Ma E and Chen M W 2001 *Appl. Phys. Lett.* **80** 2395-97
[7]   Valiev R Z 2003 *Adv. Eng. Mater.* **5** 296-300
[8]   Ma E 2006 *J. Miner. Met. Mater. Soc.* **58** 49-53
[9]   Stolyarov V V, Zhu Y T, Lowe T C and Valiev R Z 2001 *Mater. Sci. Eng.* A **303** 82-9
[10]   Krasilnikov N, Lojkowski W, Pakiela Z and Valiev R 2005 *Mater. Sci. Eng.* A **397** 330-7
[11]   Shrivastava S C, Jonas J J and Canova G 1982 *J. Mech. Phys. Solids* **30** 75-90
[12]   Wang Y M, Wang K, Pan D, Lu K, Hemker K J and Ma E 2003 *Scr. Mater.* **48** 1581-6
[13]   Verlinden B, Driver J, Samajdar I and Doherty R D 2007 *Thermo-mechanical processing of metallic materials* (Oxford, UK: Elsevier Pergamon Materials Series)
[14]   Chan K S 1990 *Scr. Metall. Mater.* **24** 1725-30
[15]   Valiev R Z, Kozlov E V, Ivanov Y F, Lian J, Nazarov A A and Baudelet B 1994 *Acta Metall. Mater.* **42** 2467-75
[16]   Ko Y G, Shin D H, Park K -T and Lee C S 2006 *Scr. Mater.* **54** 1785-9
[17]   Tucker G J and McDowell D L 2011 *Int. J. Plast.* **27** 841-57